HHS Public Access

Author manuscript

Nano Lett. Author manuscript; available in PMC 2019 July 08.

Published in final edited form as:

Nano Lett. 2019 June 12; 19(6): 3878–3885. doi:10.1021/acs.nanolett.9b01057.

Small alkaline-earth-based core/shell nanoparticles for efficient upconversion

Stefan Fischer[1,*], **Randy D. Mehlenbacher**[1], **Alice Lay**[2], **Chris Siefe**[1], **A. Paul Alivisatos**[3,4,5,6], and **Jennifer A. Dionne**[1,*]

[1]Department of Materials Science and Engineering, Stanford University, 496 Lomita Mall, Stanford, CA 94305, USA

[2]Department of Applied Physics, Stanford University, 348 Via Pueblo Mall, Stanford, CA 94305, USA

[3]Materials Sciences Division, Lawrence Berkeley National Laboratory, Berkeley, California 94720, USA

[4]Department of Chemistry, University of California Berkeley, Berkeley, California 94720, USA

[5]Department of Materials Science and Engineering, University of California Berkeley, Berkeley, California 94720, USA

[6]Kavli Energy NanoScience Institute, Berkeley, California 94720, USA

Abstract

The optical efficiency of lanthanide-based upconversion is intricately related to the crystalline host lattice. Different crystal fields interacting with the electron clouds of the lanthanides can significantly affect transition probabilities between the energy levels. Here, we investigate six distinct alkaline-earth rare-earth fluoride host materials ($M_{1-x}Ln_xF_{2+x}$, MLnF) for infrared-to-visible upconversion, focusing on nanoparticles of CaYF, CaLuF, SrYF, SrLuF, BaYF, and BaLuF doped with Yb^{3+} and Er^{3+}. We first synthesize ~5 nm upconverting cores of each material via a thermal decomposition method. Then we introduce a dropwise hot-injection method to grow optically inert MYF shell layers around the active cores. Five distinct shell thicknesses are considered for each host material, resulting in 36 unique, monodisperse upconverting nanomaterials each with size below ~15nm. The upconversion quantum yield (UCQY) is measured for all core/shell nanoparticles as function of shell thickness and compared with hexagonal (β-phase) $NaGdF_4$, a traditional upconverting host lattice. While the UCQY of core nanoparticles is below the detection limit ($<10^{-5}$%), it increases by four to five orders of magnitude as the shell thickness approaches 4–6 nm. The UCQY values of our cubic MLnF nanoparticles meet or exceed the β-$NaGdF_4$ reference sample. Across all core/shell samples, SrLuF nanoparticles are the most efficient, with UCQY values of 0.53% at 80 W/cm^2 for cubic

[*]**Corresponding Author:** stfi@stanford.edu, jdionne@stanford.edu.

Author Contributions

The manuscript was written through contributions of all authors. All authors have given approval to the final version of the manuscript.

Supporting Information. Experimental details, synthesis protocols, doping level calculations, discussion on equivalent vs cation doping, TEM images, size distributions, XRD, time-dependent photoluminescence, absorption correction for UCQY, and power-dependent UCQY. This material is available free of charge via the Internet at http://pubs.acs.org.

nanoparticles with ~11 nm edge length. This efficiency is 5 times higher than our β-$NaGdF_4$ reference material with comparable core size and shell thickness. Our work demonstrates efficient and bright upconversion in ultra-small alkaline-earth-based nanoparticles, with applications spanning biological imaging and optical sensing.

Graphical Abstract

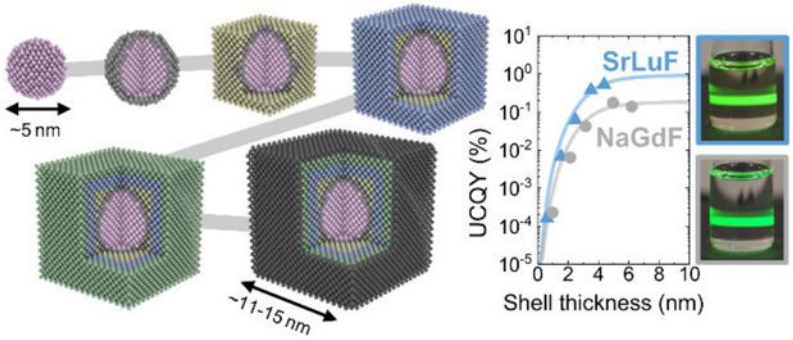

Keywords

upconversion; nanoparticles; core/shell; alkaline-earth metals

The crystalline host material of lanthanide-based luminescent materials plays a vital role in their spectroscopic properties and optical conversion efficiency. Because the interaction of 4f electrons with the crystal field of a host material is small, the energy levels of trivalent lanthanide ions are largely unchanged. However, this small interaction can significantly alter the probability of transitions between energy levels by relaxing the selection rules for radiative transitions.[1] Exploring novel host materials has led to breakthroughs in LED phosphors with higher conversion efficiencies, temperature stability, and much desired bright and narrow (~50 nm) red emission bands.[2–5] The host material has not yet played such a dominant role in research related to upconverting nanoparticles (UCNPs), where multiple low energy photons are converted into one or more higher-energy photons. Indeed, for the past decade, hexagonal-phase sodium rare-earth tetrafluoride (β-$NaLnF_4$) has served as the preeminent UCNP host material.[6–9] This host lattice is known to support relatively low phonon energies as well as two different lattice sites for the lanthanide ions which experience different crystal fields;[7] accordingly, it sustains highest upconversion quantum yields (UCQYs). The synthesis of β-$NaLnF_4$ nanoparticles is now well-understood and many syntheses as well as shelling procedures have been developed to obtain high quality and monodisperse UCNPs with different shapes and complex multiple shell layers.[10–15] Accordingly, most attention has been given to optimizing the doping concentrations of optically-active dopants[16–20], creating various nanoparticle morphologies[12,13,21,22], and coating the nanoparticle with multiple optically-inert[11,23–25] or active shells[10,14,26].

Recently, other fluoride host materials have received increasing attention, inspired in part by bulk powder studies.[19,20,22,27–31] For example, $LiLnF_4$ has received interest because of strong ultraviolet emission in core/shell UCNPs when doped with Yb^{3+} and Tm^{3+}, which

can be used for photodynamic therapy and to initiate drug release.[32] Lanthanide fluoride (LnF_3)[22,31] and lanthanide-doped alkaline fluoride (MF_2)[33–35] nanoparticles have been researched intensively but the reported upconversion efficiencies have been lower compared to the β-$NaLnF_4$. Alkaline-earth rare-earth fluoride ($M_{1-x}Ln_xF_{2+x}$) host lattices, with upconversion studies dating back to 1969,[36] promise high radiative efficiencies. For example, in bulk studies, $BaYF_5$ powder was found to have UC power conversion efficiencies rivaling GaP LEDs[37] and monocrystalline Er^{3+}-doped BaY_2F_8 showed efficient utilization of sub-bandgap photons for silicon solar cells[38]. The interchangeability of alkaline-earth and rare-earth elements in the $M_{1-x}Ln_xF_{2+x}$ system also promises tunable stoichiometry, alloying, and potentially cation doping or exchange with other elements, such as transition metal ions, to alter material and optical properties. A recent study produced monodisperse core/shell Sr_2LuF_7 UCNPs for multimodal bioimaging with bright upconversion but without any quantitative optical measurements.[39] The synthesis of $M_{1-x}Ln_xF_{2+x}$ core and core/shell nanoparticles has proven challenging, generally producing nanoparticles with broad size distributions, large variations in doping concentrations, and limited colloidal stability.[28,40–43] Moreover, $M_{1-x}Ln_xF_{2+x}$ core/shell nanoparticle performance in comparison to traditional upconverting host materials, such as β-$NaGdF_4$, remains unknown.

Here, we synthesize and characterize ultra-small $M_{1-x}Ln_xF_{2+x}$ core/shell UCNPs and benchmark their upconversion quantum yield (UCQY) and time-dependent luminescence as a function of shell thickness against the standard material system, β-$NaGdF_4$. We consider UCNPs across the alkaline-earth series (M = Ca, Sr, and Ba) in combination with Y^{3+} and Lu^{3+} as host materials for the dopants Yb^{3+} and Er^{3+}. Our alkaline-earth-based UCNPs show mostly green and red upconversion emission under 980 nm laser illumination as illustrated by the energy level diagram in Figure 1a. The dominant upconversion mechanism is based on Förster resonant energy transfer (FRET), which depends on the inverse distance between the dopants to the power of 6. Therefore, the dynamics of the non-linear upconversion processes and consequently the optical properties of the UCNPs depend significantly on the distance between the dopants.

We match the average distance between dopants of face-centered cubic-phase $M_{1-x}Ln_xF_{2+x}$ to β-$NaGdF_4$ with 20% Yb^{3+} and 2% and Er^{3+}, where the highest UCQY values have been reported.[7,9] For a given crystal structure and lattice parameters, the average distance translates to an equivalent doping concentration, which we use for the synthesis of the $M_{1-x}Ln_xF_{2+x}$ UCNPs. The alkaline-earth rare-earth fluoride (MLnF) material system is based on the MF_2 crystal structure and every alkaline-earth cation position can be exchanged with rare-earth cations. This cation interchangeability makes the $M_{1-x}Ln_xF_{2+x}$ quite complex but also very interesting and versatile. A detailed discussion on equivalent doping of rare-earth cations versus all cations, M and Ln, is given in the Supporting Information (SI). In the following, we use the abbreviations MLnF for $M_{1-x}Ln_xF_{2+x}$ and NaGdF for β-$NaGdF_4$.

The six different MLnF UCNP core samples - CaYF, CaLuF, SrYF, SrLuF, BaYF, and BaLuF – are synthesized by thermal decomposition of alkaline-earth (M) and rare-earth (Ln) trifluoroacetate salts in a 1:1 molar ratio in oleic acid (OA), 1-octadecene (ODE), and oleylamine (OLA) at 300°C under inert atmosphere using a Schlenk line. We adopt this core

synthesis from a recent report of monodisperse Sr_2LuF_7 UCNPs (see SI).[39] We target doping concentrations of 28.4% Yb^{3+} and 2.8% Er^{3+} based on equivalent doping considerations. We then develop a hot injection shelling method to grow the corresponding inert MYF layers around the upconverting cores. The cores are shelled by dropwise injection of shelling precursor solutions into the 300°C mixture of washed UCNP cores in OA and ODE (see Figure 1b). Yttrium oleate and alkaline-earth trifluoroacetate salts dissolved in OA and ODE are mixed with a 1:1 molar ratio and used as shelling precursor solutions. Using the core diameter, we calculated the amount of shell precursor to be added to obtain shell thicknesses of 1, 2, 3, 5, and 7 nm. After injection of the corresponding shell precursor amount, we wait 5 min before taking an aliquot using a glass syringe and continuing the shelling procedure for the next sample. The NaGdF core and core/shell UCNPs are prepared as reported in literature,[25] apart from washing the core UCNPs before shelling to reduce possible intermixing due to potentially unconsumed rare-earth cations in the core synthesis mixture. All UCNPs are dispersed in toluene for characterization.

TEM images of our UCNP cores are shown in Figure 1c–i. The cores are monodisperse and around 5 nm in diameter. During the shelling procedure of each MLnF combination, we extract aliquots at different times to obtain a series of five core/shell UCNP samples (CS1-CS5). The UCNPs with the thickest shell (CS5) are shown in Figure 1 j–p, while CS1-CS4 are shown in the SI. All samples are of high crystalline quality and monodisperse with standard deviation around 10%. The measured shell thicknesses vary between the samples due to uncertainty in the core diameter, unequal amounts of aliquots taken out of the hot solution, and varying stoichiometric ratios of the different MLnF UCNPs. Detailed material characterization and distributions of all samples are compiled in the SI. Shape transformation from spherical to cubic is observed after the first or second aliquot when the nanoparticle size exceeds approximately 7 nm. Ca-based nanoparticles, however, remain more spherical. This morphology could be related to a kinetically-dominated shell growth regime, due to the lower decomposition temperature of Ca trifluoroacetate compared to the other alkaline-earth trifluoroacetates. To compare the cubic-morphology MLnF samples to the spherical NaGdF particles, we calculate an effective diameter by equating the cube volume to a spherical volume (see SI). For example, the sample SrLuF CS5 with edge length of 11±1 nm converts into an effective diameter of 13.6±1.2 nm (see SI).

We use X-ray powder diffraction (XRD) to assign all MLnF samples to face-centered cubic structure with space group Fm-3m. We note, however, that reference XRD patterns are at similar positions for a large variation of M:Ln stoichiometric ratios as well as different crystal structures.[28,41,44] Therefore, our samples may contain different phases as well (see SI). As an example, the XRD patterns of SrLuF core and core/shell samples are shown Figure 2a. The line broadening due to the small size of the nanoparticles decreases with increasing shell thickness due to the larger overall size of the UCNPs. The XRD pattern of all CS5 samples are shown in Figure 2b. The XRD peaks shift towards lower diffraction angles for heavier alkaline-earth elements in the MLnF host lattice because of the smaller lattice parameters. In the case of CS5, the XRD patterns are dominated by the shell material, which contributes up to 25 times more material to the CS5 UCNP than the active core.

We measure the composition of the core UCNPs by inductively coupled plasma optical emission spectroscopy (ICP-OES) and find the ratio between the rare-earth ions of Yb^{3+} and Er^{3+} in the Lu-based hosts are around 31% and 2.8%, close to our targeted values of 28.4% and 2.8%. The Y-based samples have significantly lower doping around 23% and 2.3% (see Table 1).

UCNPs are dispersed in toluene to form transparent solutions and produce bright upconversion luminescence, seen in Figure 3a. The color of the UC emission changes due to different contributions from the green ($^2H_{11/2}$, $^4S_{3/2}$)$\rightarrow$$^4I_{15/2}$ and red $^4F_{9/2}\rightarrow{}^4I_{15/2}$ Er^{3+} transitions, evidenced by changes to the relative green and red intensities in upconversion spectra (Figure 3b). In comparison to the NaGdF reference, all MLnF samples show stronger red emission. We measured the upconversion quantum yield (UCQY) as a function of irradiance and shell thickness using 980 nm continuous-wave (cw) laser excitation. The UCNPs also emit around 980 nm from Er^{3+} $^4I_{11/2}\rightarrow{}^4I_{15/2}$ and Yb^{3+} $^2F_{5/2}\rightarrow{}^2F_{7/2}$ transitions which overlaps with the laser excitation. We subtract this emission in our UCQY analysis to accurately estimate the UCQY values (see SI). The UCQY of all cores was below our setup's detection limit of ~10^{-5}%.

Typically, thicker shells increase UCQY values by reducing surface quenching effects, which can be minimized at shell thicknesses of 4–10 nm.[25,45–48] For a meaningful comparison between the samples, we factor out the effect of shell thickness by fitting the data to a simple model described by Equation 1.[47,49] The effect of surface quenching can be described by Förster-type energy transfer from a donor to a plane acceptor, the surface, by

$$UCQY(d) = \frac{UCQY(d \rightarrow \infty)}{1 + (d_0/d)^4}. \quad (1)$$

Here, d is the shell thickness, d_0 is the Förster distance, and UCQY($d\rightarrow\infty$) is the UCQY for infinite thick shells; d_0 and UCQY($d\rightarrow\infty$) are fitting parameters.[46,47] Figure 3c shows the UCQY trend as a function of shell thickness for an irradiance of 80 W/cm^2. We find excellent agreement between our data and fits using Equation 1. Importantly, the UCQY of all samples is enhanced by more than 4 orders of magnitude upon shelling, demonstrating the enormous beneficial effect of surface passivation in ultra-small UCNPs. As seen, the MLuF samples are generally more efficient than the MYF ones, which may be related to the closer value of the cation doping concentration to the hypothesized optimum in MLnF. SrLuF is the most efficient upconverter with an UCQY of 0.53±0.07% at 80 W/cm^2 for nanoparticles with an edge length of 11.0±1.0 nm. This efficiency translates into an enhancement of >52,800× from the SrLuF cores of 4.9±0.4 nm in diameter to core/shell UCNPs with thickest shell, considering our UCQY detection limit of ~10^{-5}% for the core UCNPs. Accordingly, the UCQY($d\rightarrow\infty$) is >94,300× higher than the core UCQY value.

The UCQY of all samples is far from saturation and higher efficiencies can be reached at higher irradiances (Figure 3d). The NaGdF UCQY values as well as the enhancement factors from the core to the core/shell CS5 presented in this study are similar to reported values for comparable core/shell UCNPs in literature.[25] Surprisingly, we found that the NaGdF sample

is the least efficient upconverter in our definition of UCQY($d\rightarrow\infty$) (Figure 3e). All MLnF UCNPs have much more efficient red emission than NaGdF but only SrLuF shows also more efficient green emission than NaGdF. The UCQY($d\rightarrow\infty$) value of the SrLuF samples is 5× higher than the NaGdF reference.

It is well known that increasing the size of the core significantly enhances the UCQY values in core-only as well core/shell UCNPs.[25,46,50] Therefore, it is important to compare UCNPs with same core size and shell thickness. There are very few reports on UCQY values for ultra-small core/shell UCNPs. The most comparable studies with similar core size and shell thickness are from Li et al., Hudry et al, and Würth et al (see also SI).[23,25,48] Li et al. reported an UCQY of 0.5% at 100 W/cm^2 for ~5 nm β-$NaYF_4$: 20% Yb^{3+}, 2% Er^{3+} core with ~6 nm β-$NaYF_4$ shell with a total diameter of 17nm.[23] Hudry et al. determined an UCQY of ~0.55% at 100 W/cm^2 for ~4.8 nm β-$NaGdF_4$: 20% Yb^{3+}, 2% Er^{3+} core with ~3.5 nm β-$NaYF_4$ shell with a total diameter of 11.7nm.[48] Würth et al. measured an UCQY of ~0.3% at 100 W/cm^2 for ~4 nm β-$NaGdF_4$: 20% Yb^{3+}, 2% Er^{3+} core with ~6 nm β-$NaYF_4$ shell with a total diameter of 16nm.[25] To be comparable to the literature values, we estimate an UCQY for our SrLuF CS5 sample of 0.66% at 100 W/cm^2 by extrapolating the irradiance-dependent UCQY shown in Figure 3d. In order to account for the thicker inert shell layers reported by Li et al. and Würth et al., we extrapolate to a shell thickness of ~5.5 nm using the data shown in Figure 3c and Figure 3d. For such SrLuF core/shell UCNPs with a total size of ~16 nm, we estimate an UCQY of ~1.0% at 100 W/cm^2. This comparison shows that our SrLuF core/shell UCNPs are as efficient or even better than the best β-$NaLnF_4$ core/shell UCNPs found in literature when considering equivalent core size, shell thickness, and irradiance. The excellent efficiency of SrLuF is based on equivalent doping considerations to equal β-$NaGdF_4$ with 20% Yb^{3+} and 2% Er^{3+}. The concept of equivalent doping is a reasonable starting point for our investigation of MLnF UCNPs but it is a simplification of the dopant distribution in the crystals. Moreover, it does not account for changes in stoichiometric ratios between the alkaline-earth and the rare-earth cations (see SI). It is expectable that higher UCQY values are possible by optimizing the concentration of the dopants.

We next measure time-dependent luminescence of the most relevant energy levels for direct photoluminescent excitation as well as in upconversion mode using 980 nm excitation for all samples (see SI). As one example, Figure 4a shows the increase of decay time from the core to the core/shell SrLuF samples for the Yb^{3+} $^2F_{5/2}\rightarrow{}^2F_{7/2}$ transition. The decay curves of the CS5 samples of all considered host lattices are shown in Figure 4b–d under 980 nm excitation and emission of the Yb^{3+} $^2F_{5/2}\rightarrow{}^2F_{7/2}$ transition at 1000 nm, Er^{3+} $^2S_{3/2}\rightarrow{}^4I_{15/2}$ transition at 540 nm, and Er^{3+} $^4F_{9/2}\rightarrow{}^4I_{15/2}$ transition at 654 nm, respectively. We use a 1/e definition to determine the decay times and quantify the time-dependent photoluminescence dynamics. It is often presumed that longer lifetimes of the sensitizer excited state, here Yb^{3+} $^2F_{5/2}$ (Figure 4b), translates into higher UCQY. We did not find a direct correlation between the trend in the decay time of the Yb^{3+} excited state and the UCQY. For instance, if we take CS5 samples, BaLuF is more efficient than SrYF although the lifetime of the Yb^{3+} excited state is 3 times shorter. The different crystal fields acting on the electron clouds of lanthanide ions in the different host materials may contribute to this effect of shorter lifetimes and higher efficiency by further relaxing the selection rules of certain transitions,

thereby enhancing dipole moments. Altered energy transfer rates between the lanthanides due to changes in the overlap integral of absorption and emission spectra between ground and excited states but also between excited states may be another factor for the great performance of the SrLuF sample.

It is worth noting that the rise time of the upconversion luminescence of NaGdF, shown in Figure 4c and Figure 4d, is the only one to stand out as the longest although the decay time of the Yb^{3+} $^2F_{5/2} \rightarrow {}^2F_{7/2}$ transition, shown in Figure 4b, is among the three shortest (see also SI). The shorter rise time of MLnF UCNPs may be attributed to a faster depopulation of the Er^{3+} $^2S_{3/2}$ energy level or a stronger coupling between the Yb^{3+} and Er^{3+} which could eventually lead to the higher UCQY values measured in this study for MLnF UCNPs.

To factor out the different shell thicknesses, we fit the decay times as a function of shell thickness for all material combinations with

$$\tau(d) = \frac{\tau(d \rightarrow \infty)}{1 + (d_0/d)^4} \quad (2)$$

in accordance with Equation 1. Here, we set the starting value of the function to the decay time of the core UCNPs. The trends in Figure 4e are different to the ones of the UCQY in Figure 3c further highlighting the discrepancy between decay time and UCQY in different host materials. While in Figure 3c Lu-based and Y-based MLnF UCNPs build separate groups, in Figure 4e the different alkaline-earth elements seem to build groups; Ba-based samples show the shortest decay time, Sr-based samples have the longest decay time, and Ca-based samples are in the middle.

To further quantify the differences in the host materials, the same data analysis is performed on the time-dependent luminescence under direct excitation of the measured energy level at center emission wavelength of 540 nm, 654 nm, 1000 nm, and 1530 nm to obtain the $\tau(d \rightarrow \infty)$ values relative to those of NaGdF (Figure 4f). In general, the Er^{3+} $^4S_{3/2}$ energy level in MLnF UCNPs have significantly shorter lifetimes in contrast to NaGdF. The reddest samples, CaYF and CaLuF, also have shorter Er^{3+} $^4F_{9/2}$ lifetimes suggesting larger dipole moments likely as a result of different crystal field distortion of the electron cloud of erbium ions. The NIR emission from Er^{3+} $^4I_{13/2} \rightarrow {}^4I_{15/2}$ is quite similar for all samples with ~20% longer decay times for the Sr- and Ba-based samples.

The superior performance of SrLuF could be explained by several factors, including relaxed selection rules, modified phonon modes, or reduced cation intermixing. Detailed spectroscopic analysis including Judd-Ofelt theory could provide insight into the dipole moments of the transitions. Additionally, determining the phonon energy distribution and FRET rates between different energy levels could inform the dynamics of upconversion between the different materials. Finally, we note that cation intermixing at the core/shell interface impacts the performance of the UCNPs. In particular, mixing of rare-earth ions from core and shell layers due to diffusion or incorporation during the shelling procedure can reduce the passivation effect of the shell layer and dilute the active cations in the core.

[25,48] The superior performance of SrLuF may be a result of less pronounced cation intermixing compared to other host materials such as NaGdF. All such studies are exciting future directions to explore in pursuit of the next high-efficiency upconverting host.

In conclusion, we have introduced a host material platform for efficient and small lanthanide-doped core/shell nanoparticles. We have synthesized a series of ~5nm alkaline-earth rare-earth fluoride (MLnF) core UCNPs and developed a hot-injection shelling approach. Inert MYF shell layers with different thickness have been grown around the active cores of the 6 different MLnF UCNPs. We compared the optical properties of the different MLnF UCNPs to β-$NaGdF_4$, a reference upconverter host material, as a function of the shell thickness. Due to reduced surface quenching by the inert shell layers, we measured efficiency enhancements of 4–5 orders of magnitude from the core to the core/shell samples. The host material SrLuF provides the most efficient UCNPs of the samples studied and outperforms the β-$NaGdF_4$ reference by a factor of 5 at comparable core sizes and shell thickness. Our SrLuF is also as efficient or better than comparable $NaYF_4$-based UCNPs reported in the literature. Further optimization of doping concentrations for the alkaline-earth rare-earth fluoride host materials promise even better performance with higher UCQY and brightness. In addition, the interchangeability of alkaline-earth and rare-earth elements in the MLnF system allow strong variations in stoichiometric ratios, alloying, and potentially cation doping or exchange with other elements, such as transition metal ions, to alter material and optical properties. Our results show that MLnF, and in particular SrLuF, are host materials that provide efficient upconversion for ultra-small UCNPs, which are particularly interesting as multiphoton nanoprobes for applications in biological imaging and sensing, life science and energy-related applications.

Supplementary Material

Refer to Web version on PubMed Central for supplementary material.

ACKNOWLEDGMENT

The authors would like to thank Claire McLellan for scientific feedback. This work is part of the ‘Photonics at Thermodynamic Limits’ Energy Frontier Research Center funded by the U.S. Department of Energy, Office of Science, Office of Basic Energy Sciences under Award Number DE-SC0019140. A.L. and J.A.D. also acknowledge support from NIH grant 5R21GM129879–02 and C.S. acknowledges support from an Eastman Kodak Fellowship. TEM imaging and XRD characterization was performed at the Stanford Nano Shared Facilities (SNSF), supported by the National Science Foundation under award ECCS-1542152. All opinions expressed in this paper are the authors’ and do not necessarily reflect the policies and views of NSF, DOE, and Stanford University.

Funding Sources

DOE EFRC under Award Number DE-SC0019140; NIH grant 5R21GM129879–02;

ABBREVIATIONS

UCNP	upconverting nanoparticles
UCQY	upconversion quantum yield
Ln	rare-earth metals

M	alkaline-earth metals
NaGdF	β-$NaYF_4$
MLnF	$M_{1-x}Ln_xF_{2+x}$

REFERENCES

(1). Henderson B; Imbusch GF Optical Spectroscopy of Inorganic Solids; Oxford University Press, 2006; Vol. 3.

(2). Pust P; Weiler V; Hecht C; Tücks A; Wochnik AS; Henß A-K; Wiechert D; Scheu C; Schmidt PJ; Schnick W Narrow-Band Red-Emitting Sr[LiAl3N4]:Eu2+ as a next-Generation LED-Phosphor Material. Nat. Mater 2014, 13 (9), 891–896. [PubMed: 24952748]

(3). Wang Z; Ha J; Kim YH; Bin Im W; McKittrick J; Ong SP Mining Unexplored Chemistries for Phosphors for High-Color-Quality White-Light-Emitting Diodes. Joule 2018, 2 (5), 914–926.

(4). Maak C; Strobel P; Weiler V; Schmidt PJ; Schnick W Unprecedented Deep-Red Ce3+ Luminescence of the Nitridolithosilicates Li38.7RE3.3Ca5.7 [Li2 Si30N59]O2F (RE = La, Ce, Y). Chem. Mater 2018, 30 (15), 5500–5506.

(5). Xia Z; Meijerink A Ce3+-Doped Garnet Phosphors: Composition Modification, Luminescence Properties and Applications. Chem. Soc. Rev 2017, 46 (1), 275–299. [PubMed: 27834975]

(6). Huang X; Han S; Huang W; Liu X Enhancing Solar Cell Efficiency: The Search for Luminescent Materials as Spectral Converters. Chem. Soc. Rev 2013, 42 (1), 173–201. [PubMed: 23072924]

(7). Goldschmidt JC; Fischer S Upconversion for Photovoltaics - a Review of Materials, Devices and Concepts for Performance Enhancement. Adv. Opt. Mater 2015, 3 (4), 510–535.

(8). Chen X; Peng D; Ju Q; Wang F Photon Upconversion in Core–shell Nanoparticles. Chem. Soc. Rev 2015, 44 (6), 1318–1330. [PubMed: 25058157]

(9). Wilhelm S Perspectives for Upconverting Nanoparticles. ACS Nano 2017, 11 (11), 10644–10653. [PubMed: 29068198]

(10). Vetrone F; Naccache R; Mahalingam V; Morgan CG; Capobianco JA The Active-Core/Active-Shell Approach: A Strategy to Enhance the Upconversion Luminescence in Lanthanide-Doped Nanoparticles. Adv. Funct. Mater 2009, 19 (18), 2924–2929.

(11). Johnson NJJ; Korinek A; Dong C; Van Veggel FCJM Self-Focusing by Ostwald Ripening: A Strategy for Layer-by-Layer Epitaxial Growth on Upconverting Nanocrystals. J. Am. Chem. Soc 2012, 134, 11068–11071. [PubMed: 22734596]

(12). Liu D; Xu X; Du Y; Qin X; Zhang Y; Ma C; Wen S; Ren W; Goldys EM; Piper JA; et al. Three-Dimensional Controlled Growth of Monodisperse Sub-50 Nm Heterogeneous Nanocrystals. Nat. Commun 2016, 7, 10254. [PubMed: 26743184]

(13). Fischer S; Swabeck JK; Alivisatos AP Controlled Isotropic and Anisotropic Shell Growth in β-NaLnF4 Nanocrystals Induced by Precursor Injection Rate. J. Am. Chem. Soc 2017, 139 (35), 12325–12332. [PubMed: 28777550]

(14). Xie X; Gao N; Deng R; Sun Q; Xu Q-H; Liu X Mechanistic Investigation of Photon Upconversion in Nd3+-Sensitized Core–Shell Nanoparticles. J. Am. Chem. Soc 2013, 135 (34), 12608–12611. [PubMed: 23947580]

(15). Hao S; Chen G; Yang C; Shao W; Wei W; Liu Y; Prasad PN Nd3+-Sensitized Multicolor Upconversion Luminescence from a Sandwiched Core/Shell/Shell Nanostructure. Nanoscale 2017, 9 (30), 10633–10638. [PubMed: 28656192]

(16). Gargas DJ; Chan EM; Ostrowski AD; Aloni S; Altoe MVP; Barnard ES; Sanii B; Urban JJ; Milliron DJ; Cohen BE; et al. Engineering Bright Sub-10-Nm Upconverting Nanocrystals for Single-Molecule Imaging. Nat. Nanotechnol 2014, 9 (4), 300–305. [PubMed: 24633523]

(17). Fischer S; Fröhlich B; Krämer KW; Goldschmidt JC Relation between Excitation Power Density and Er3+ Doping Yielding the Highest Absolute Upconversion Quantum Yield. J. Phys. Chem. C 2014, 118 (51), 30106–30114.

(18). Ma C; Xu X; Wang F; Zhou Z; Liu D; Zhao J; Guan M; Lang CI; Jin D Optimal Sensitizer Concentration in Single Upconversion Nanocrystals. Nano Lett 2017, 17 (5), 2858–2864. [PubMed: 28437117]

(19). Tian B; Fernandez-Bravo A; Najafiaghdam H; Torquato NA; Altoe MVP; Teitelboim A; Tajon CA; Tian Y; Borys NJ; Barnard ES; et al. Low Irradiance Multiphoton Imaging with Alloyed Lanthanide Nanocrystals. Nat. Commun 2018, 9 (1), 3082. [PubMed: 30082844]

(20). Wen S; Zhou J; Zheng K; Bednarkiewicz A; Liu X; Jin D Advances in Highly Doped Upconversion Nanoparticles. Nat. Commun 2018, 9 (1), 2415. [PubMed: 29925838]

(21). Li Z; Zhang Y An Efficient and User-Friendly Method for the Synthesis of Hexagonal-Phase NaYF4:Yb, Er/Tm Nanocrystals with Controllable Shape and Upconversion Fluorescence. Nanotechnology 2008, 19 (34), 345606. [PubMed: 21730655]

(22). Naccache R; Yu Q; Capobianco JA The Fluoride Host: Nucleation, Growth, and Upconversion of Lanthanide-Doped Nanoparticles. Adv. Opt. Mater 2015, 3 (4), 482–509.

(23). Li X; Shen D; Yang J; Yao C; Che R; Zhang F; Zhao D Successive Layer-by-Layer Strategy for Multi-Shell Epitaxial Growth: Shell Thickness and Doping Position Dependence in Upconverting Optical Properties. Chem. Mater 2013, 25, 106–112.

(24). Naduviledathu Raj A; Rinkel T; Haase M Ostwald Ripening, Particle Size Focusing, and Decomposition of Sub-10 Nm NaREF4 (RE = La, Ce, Pr, Nd) Nanocrystals. Chem. Mater 2014, 26 (19), 5689–5694.

(25). Würth C; Fischer S; Grauel B; Alivisatos AP; Resch-Genger U Quantum Yields, Surface Quenching, and Passivation Efficiency for Ultrasmall Core/Shell Upconverting Nanoparticles. J. Am. Chem. Soc 2018, 140 (14), 4922–4928. [PubMed: 29570283]

(26). Chen G; Damasco J; Qiu H; Shao W; Ohulchanskyy TY; Valiev RR; Wu X; Han G; Wang Y; Yang C; et al. Energy-Cascaded Upconversion in an Organic Dye-Sensitized Core/Shell Fluoride Nanocrystal. Nano Lett 2015, 15 (11), 7400–7407. [PubMed: 26487489]

(27). Boccolini A; Favilla E; Tonelli M; Richards BS; Thomson RR Highly Efficient Upconversion in Er3+ Doped BaY2F8 Single Crystals: Dependence of Quantum Yield on Excitation Wavelength and Thickness. Opt. Express 2015, 23 (15), A903. [PubMed: 26367690]

(28). Grzyb T; Przybylska D Formation Mechanism, Structural, and Upconversion Properties of Alkaline Rare-Earth Fluoride Nanocrystals Doped With Yb3+/Er3+ Ions. Inorg. Chem 2018, 57 (11), 6410–6420. [PubMed: 29756764]

(29). Liang H; Zheng Y; Chen G; Wu L; Zhang Z; Cao W Enhancement of Upconversion Luminescence of Y2O3:Er3+ Nanocrystals by Codoping Li+–Zn2+. J. Alloys Compd 2011, 509 (2), 409–413.

(30). Wang J; Deng R; MacDonald MA; Chen B; Yuan J; Wang F; Chi D; Andy Hor TS; Zhang P; Liu G; et al. Enhancing Multiphoton Upconversion through Energy Clustering at Sublattice Level. Nat. Mater 2013, 13 (2), 157–162. [PubMed: 24270581]

(31). Haase M; Schäfer H Upconverting Nanoparticles. Angew. Chemie Int. Ed 2011, 50 (26), 5808–5829.

(32). Cheng T; Marin R; Skripka A; Vetrone F Small and Bright Lithium-Based Upconverting Nanoparticles. J. Am. Chem. Soc 2018, 140 (40), 12890–12899. [PubMed: 30215515]

(33). Wang G; Peng Q; Li Y Upconversion Luminescence of Monodisperse CaF2:Yb3+/Er3+ Nanocrystals. J. Am. Chem. Soc 2009, 131 (40), 14200–14201. [PubMed: 19775118]

(34). Pedroni M; Piccinelli F; Passuello T; Polizzi S; Ueda J; Haro-González P; Martinez Maestro L; Jaque D; García-Solé J; Bettinelli M; et al. Water (H2O and D2O) Dispersible NIR-to-NIR Upconverting Yb3+/Tm3+ Doped MF2 (M = Ca, Sr) Colloids: Influence of the Host Crystal. Cryst. Growth Des 2013, 13 (11), 4906–4913.

(35). Quintanilla M; Cantarelli IX; Pedroni M; Speghini A; Vetrone F Intense Ultraviolet Upconversion in Water Dispersible SrF2:Tm3+,Yb3+ Nanoparticles: The Effect of the Environment on Light Emissions. J. Mater. Chem. C 2015, 3 (13), 3108–3113.

(36). Guggenheim HJ; Johnson LF New Fluoride Compunds for Efficient Infrared-to-Visible Conversion. Appl. Phys. Lett 1969, 15 (2), 51–52.

(37). Johnson LF; Guggenheim HJ; Rich TC; Ostermayer FW Infrared-to-Visible Conversion by Rare-Earth Ions in Crystals. J. Appl. Phys 1972, 43 (3), 1125–1137.

(38). Fischer S; Favilla E; Tonelli M; Goldschmidt JC Record Efficient Upconverter Solar Cell Devices with Optimized Bifacial Silicon Solar Cells and Monocrystalline BaY2F8:30% Er3+. Sol. Energy Mater. Sol. Cells 2015, 136, 127–134.

(39). Chen C; Liu J; Chen Y; Li C; Liu X; Huang H; Liang C; Lou Y; Shi Z; Feng S Sub-10 Nm Sr2LuF7:Yb/Er@Sr2GdF7@SrF2 Up-Conversion Nanocrystals for Up-Conversion Luminescence–Magnetic Resonance–Computed Tomography Trimodal Bioimaging. ACS Appl. Mater. Interfaces 2017, 9 (7), 5748–5756. [PubMed: 28170224]

(40). Vetrone F; Mahalingam V; Capobianco JA Near-Infrared-to-Blue Upconversion in Colloidal BaYF5:Tm3+, Yb3+ Nanocrystals. Chem. Mater 2009, 21 (9), 1847–1851.

(41). Grzyb T; Balabhadra S; Przybylska D; Węcławiak M Upconversion Luminescence in BaYF5, BaGdF5 and BaLuF5 Nanocrystals Doped with Yb3+/Ho3+, Yb3+/Er3+ or Yb3+/Tm3+ Ions. J. Alloys Compd 2015, 649, 606–616.

(42). Zhang Y; Liu X; Lang Y; Yuan Z; Zhao D; Qin G; Qin W Synthesis of Ultra-Small BaLuF5-:Yb3+,Er3+ @BaLuF5-:Yb3+ Active-Core–active-Shell Nanoparticles with Enhanced up-Conversion and down-Conversion Luminescence by a Layer-by-Layer Strategy. J. Mater. Chem. C 2015, 3 (9), 2045–2053.

(43). Ma M; Xu C; Yang L; Yang Q; Lin J Solvothermal Synthesis and Tailored Upconversion Emission of Monodisperse Ultrasmall Face-Centered Cubic Sr2YF7 Nanocrystals. J. Alloys Compd 2012, 525, 97–102.

(44). Favilla E; Cittadino G; Veronesi S; Tonelli M; Fischer S; Goldschmidt JC; Cassanho A; Jenssen HP Comparative Analysis of Upconversion Efficiencies in Fluoride Materials for Photovoltaic Application. Sol. Energy Mater. Sol. Cells 2016, 157, 415–421.

(45). Fischer S; Johnson NJJ; Pichaandi J; Goldschmidt JC; Van Veggel FCJM Upconverting Core-Shell Nanocrystals with High Quantum Yield under Low Irradiance: On the Role of Isotropic and Thick Shells. J. Appl. Phys 2015, 118 (19), 193105.

(46). Fischer S; Bronstein ND; Swabeck JK; Chan EM; Alivisatos AP Precise Tuning of Surface Quenching for Luminescence Enhancement in Core–Shell Lanthanide-Doped Nanocrystals. Nano Lett 2016, 16 (11), 7241–7247. [PubMed: 27726405]

(47). Hossan MY; Hor A; Luu Q; Smith SJ; May PS; Berry MT Explaining the Nanoscale Effect in the Upconversion Dynamics of β-NaYF4:Yb3+, Er3+ Core and Core–Shell Nanocrystals. J. Phys. Chem. C 2017, 121 (30), 16592–16606.

(48). Hudry D; Busko D; Popescu R; Gerthsen D; Abeykoon AMM; Kübel C; Bergfeldt T; Richards BS Direct Evidence of Significant Cation Intermixing in Upconverting Core@Shell Nanocrystals: Toward a New Crystallochemical Model. Chem. Mater 2017, 29 (21), 9238–9246.

(49). Kuhn H Classical Aspects of Energy Transfer in Molecular Systems. J. Chem. Phys 1970, 53 (1), 101–108.

(50). Boyer J-CC; van Veggel FCJM Absolute Quantum Yield Measurements of Colloidal NaYF4: Er3+, Yb3+ Upconverting Nanoparticles. Nanoscale 2010, 2 (8), 1417–1419. [PubMed: 20820726]

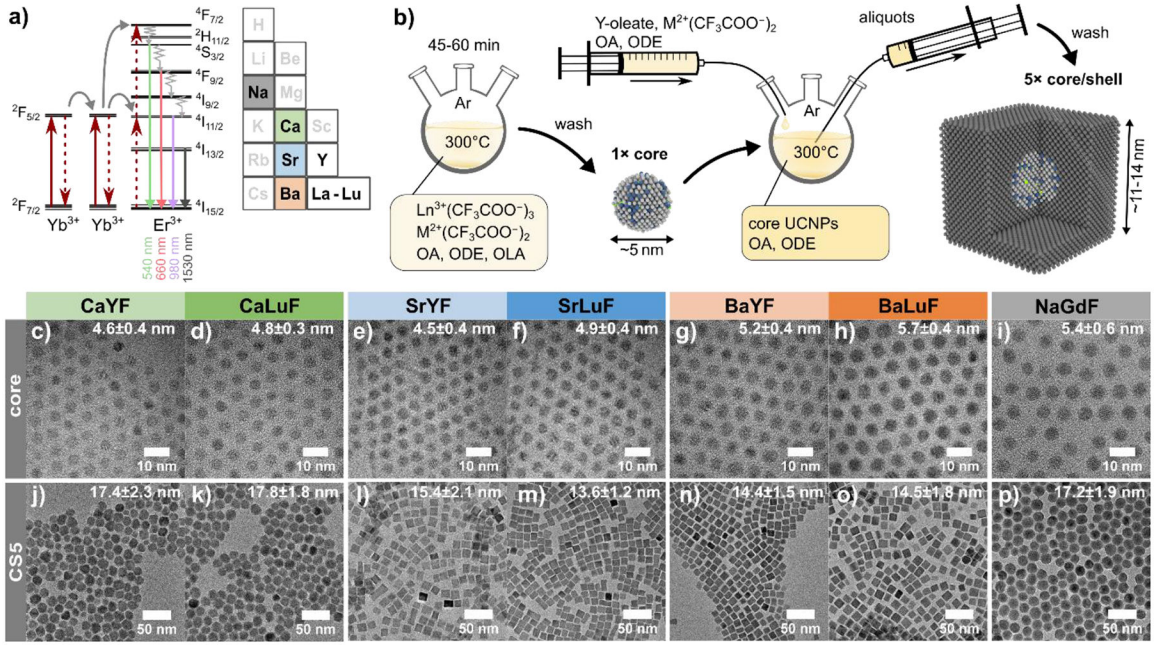

Figure 1.

a) Schematic of the energy level diagram and proposed upconversion scheme. Section of the periodic table that highlights the alkaline-earth elements (group 2) used in this study. b) Illustration of the core and core/shell synthesis for the MLnF UCNPs by decomposition of rare-earth (Ln) and alkaline-earth (M) trifluoroacetate precursors. For each host material, 5 aliquots of core/shell samples were taken with increasing shell thickness (CS1 to CS5). c-i) TEM images of the core UCNPs with size distribution and standard derivation from measuring more than 300 nanoparticles. j-p) TEM images of the core/shell UCNPs with thickest shell CS5. For UCNPs with cubic shape, the edge length was converted into a diameter to be more comparable to the diameter of the reference sample NaGdF.

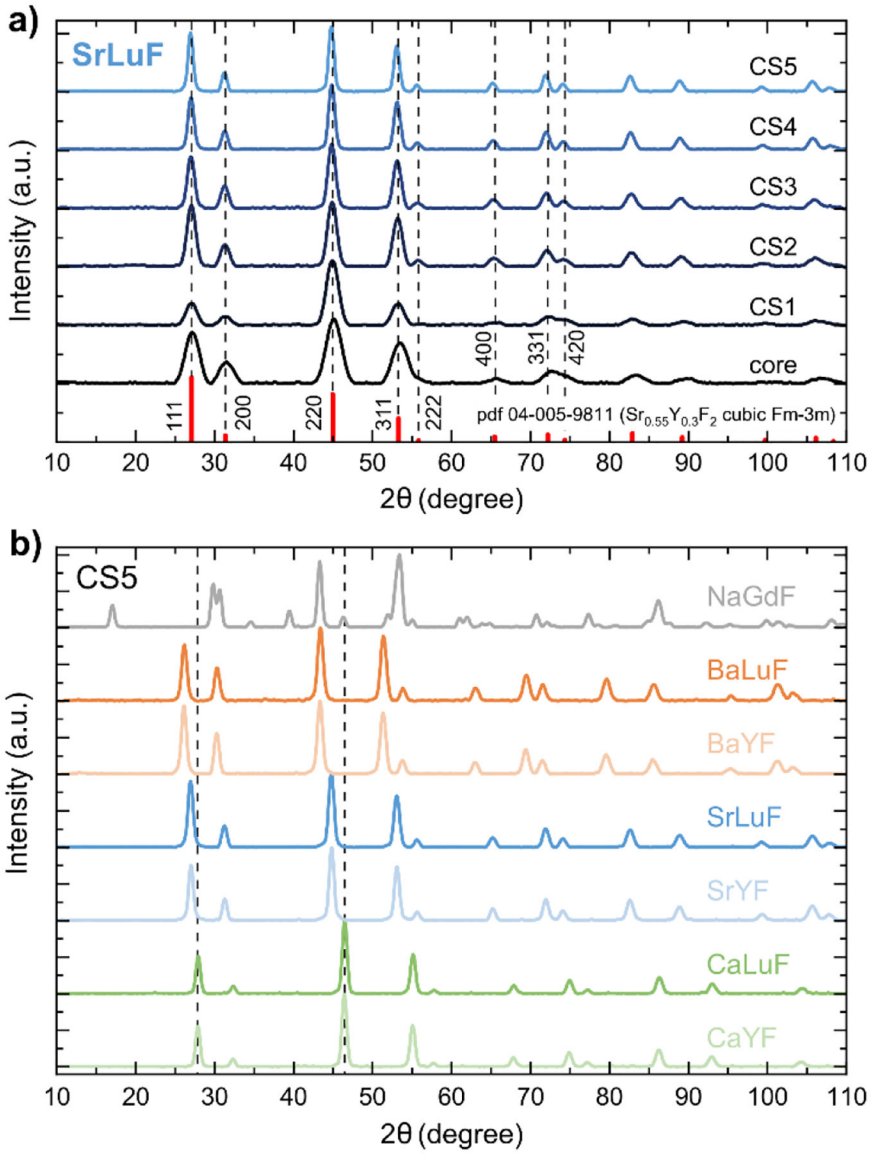

Figure 2.

a) XRD patterns of SrLuF core and core/shell samples match face-centered cubic crystal structure with space group Fm-3m. b) XRD patterns of the CS5 UCNPs in direct comparisons. All alkaline-earth rare-earth fluoride (MLnF) compounds fit best to face-centered cubic crystal structure. The heavier the alkaline-earth metals in the compounds, the shorter the lattice parameters as expressed in XRD peak shift to lower diffraction angels. The NaGdF sample shows pure hexagonal-phase.

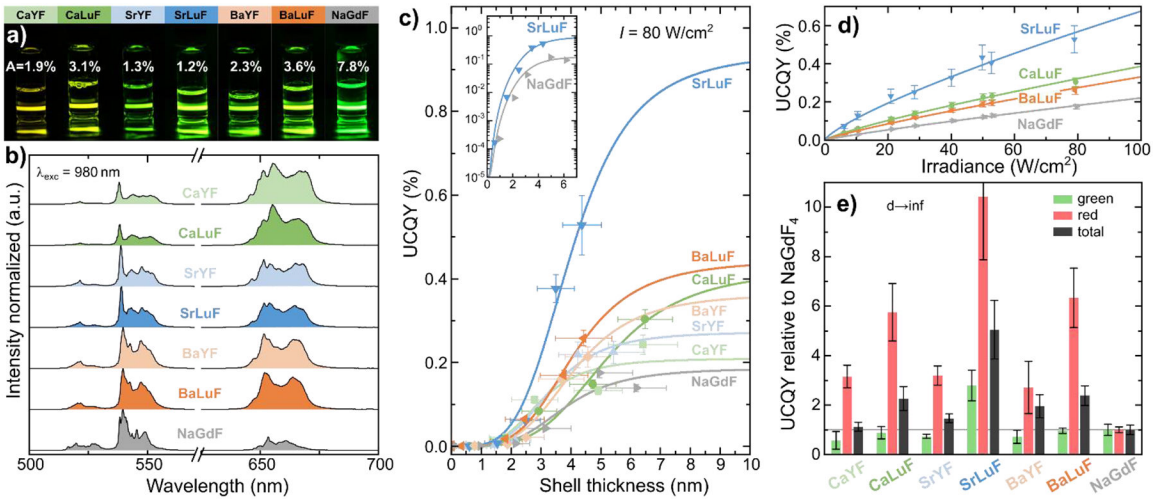

Figure 3.

a) Photographs of the core/shell (CS5) UCNPs dispersed in toluene under cw 980 nm laser excitation with irradiance of ~10 W/cm^2. The percentage numbers are the absorptance values of the solutions as determined at UCQY measurements. The higher absorptance of NaGdF is mainly caused by the higher UCNP concentraton in the solution. b) Upconversion emission spectra of the CS5 UCNP samples at 80 W/cm^2 as measured in UCQY measurements using an integrating sphere. c) UCQY of the different host materials as a function of shell thickness at 80 W/cm^2 is fitted with a FRET-type surface quenching function described by Equation 1. Enhancements of more than 4 orders of magnitude are measured for all compounds from the core to the core/shell samples. d) The UCQY as a function of irradiance shows that all samples are far from saturation meaning that higher UCQY values are achievable at higher irradiances. e) The UCQY($d\rightarrow\infty$) are normalized to the values obtained for NaGdF. All MLnF samples show stronger red emission, whereas only SrLuF also shows more efficient green emission. SrLuF outperforms the NaGdF reference by a factor of 5.

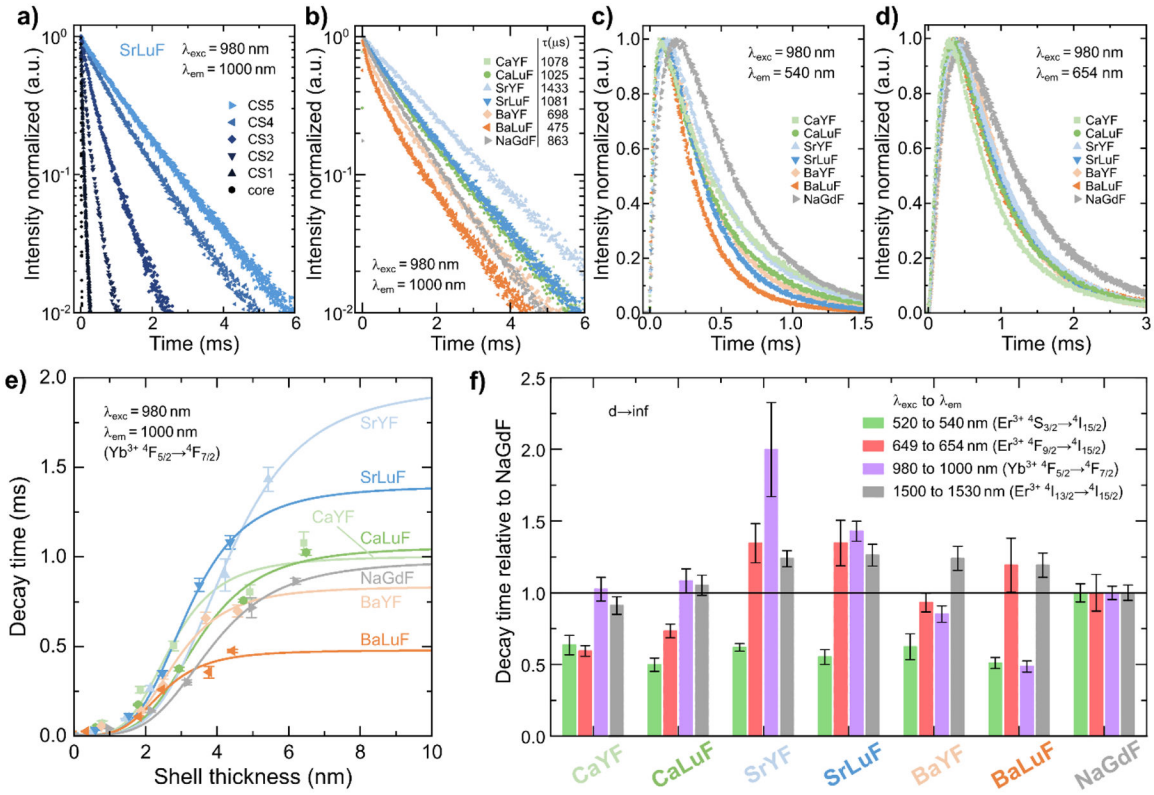

Figure 4.

a) Time-dependent luminescence of $Yb^{3+}\ {}^4F_{5/2}\rightarrow{}^4F_{7/2}$ transition using 980 nm excitation and 1000 nm detection wavelength for the SrLuF samples. Time-dependent luminescence of b) $Yb^{3+}\ {}^2F_{5/2}\rightarrow{}^2F_{7/2}$ transition at 1000 nm, c) $Er^{3+}\ {}^2S_{3/2}\rightarrow{}^4I_{15/2}$ transition at 540 nm, and d) $Er^{3+}\ {}^4F_{9/2}\rightarrow{}^4I_{15/2}$ transition at 654 nm under 980 nm excitation. e) Decay of the $Yb^{3+}\ {}^4F_{5/2}\rightarrow{}^4F_{7/2}$ transition as a function of shell thickness using a 1/e definition. The increase in decay time can be modeled well with a FRET-type surface quenching function (Equation 2) similar to the UCQY. f) Comparing the decay time $\tau(d\rightarrow\infty)$ under direct excitation of the MLnF compounds relative to NaGdF illustrates the significant differences between the compounds and the effect of different crystal fields on the transition probabilities.

Table 1.

Atomic composition between alkaline-earth ions (M = Ca, Sr, Ba) and rare-earth ions (Ln = Lu, Gd, Y, Yb, Er) of the core UCNPs as measured by inductively coupled plasma optical emission spectroscopy (ICP-OES). Ratios of alkaline-earth to rare-earth metals (M:Ln) as determined form the ICP-OES data show the large stoichiometric range in the $M_{1-x}Ln_xF_{2+x}$ material system. Cation doping of Yb^{3+} and Er^{3+} considering the sum of all M and Ln elements from ICP-EOS measurements. Calculated UCQY for infinite shell thickness ($d\rightarrow\infty$) at 80 W/cm^2 derived from Equation 1 and lower limit of the estimated enhancement factor Q compared to the core UCNPs. The decay time $\tau(d\rightarrow\infty)$ of the Yb^{3+} $^2F_{5/2}\rightarrow{}^2F_{7/2}$ transition (excitation at 980 nm, emissions at 1000 nm) was determined by fitting Equation 2 to the decay times as a function of shell thickness.

Material	Atomic composition of M and Ln ions (%)							Ratio	$x^{a)}$	Cation doping	UCQY($d\rightarrow\infty$)	$Q^{b)}$	$\tau(d\rightarrow\infty)$ $^2F_{5/2}\rightarrow{}^2F_{7/2}$
	Ca	Sr	Ba	Lu	Y	Yb	Er	M:Ln		Yb/Er (%)	(%)		(μs)
CaYF	99.6	0.4	0.0	0.0	75.3	22.4	2.2	1.69	0.37	8.3/0.8	0.21±0.03	20,990	998
CaLuF	99.7	0.3	0.0	66.7	0.1	30.3	2.9	1.83	0.35	10.7/1.0	0.43±0.09	42,300	1053
SrYF	1.9	98.1	0.0	0.0	74.1	23.6	2.3	1.51	0.40	9.4/0.9	0.27±0.03	27,400	1945
SrLuF	0.2	99.8	0.0	66.5	0.1	30.6	2.9	1.52	0.40	12.1/1.1	0.94±0.22	94,300	1391
BaYF	2.4	0.8	96.9	0.0	74.8	22.9	2.3	1.20	0.45	10.4/1.1	0.37±0.09	36,500	828
BaLuF	0.1	0.8	99.1	66.0	0.8	30.3	2.9	1.19	0.46	13.8/1.3	0.45±0.07	44,500	473
NaGdF	Na = 100			Gd = 80.0		17.9	2.1			9.3/1.1	0.19±0.04	18,700	973

a) $M_{1-x}Ln_xF_{2+x}$

b) Q = lower limit of estimated enhancement of UCQY($d\rightarrow\infty$) compared to core at ~80 W/cm^2